Materials Research. 2019; 22(6): e20190021
DOI: http://dx.doi.org/10.1590/1980-5373-MR-2019-0021

Effect of ageing time on the toughness and the corrosion properties of duplex stainless steel UNS S31803

***William Haupt*[a]*, *Luis Eduardo Silva*[a], *Tiago Falcade*[b], *Ana Camila Santos*[c], *Afonso Reguly*[d]**

[a]*Universidade de Passo Fundo, Passo Fundo, RS, Brasil*
[b]*Departamento de Química Física, Universidade Federal do Rio Grande do Sul, Bento Gonçalves, Porto Alegre, RS, Brasil*
[c]*Universidade Federal do Rio Grande do Sul, Porto Alegre, RS, Brasil*
[d]*Departamento de Metalurgia, Universidade Federal do Rio Grande do Sul, Porto Alegre, RS, Brasil*

Received: January 14, 2019; Revised: October 11, 2019; Accepted: December 12, 2019

Duplex stainless steels are materials with high mechanical strength, toughness, and corrosion resistance, properties that make them rather appealing for the application on chemical and petrochemical industries. However, the exposure of such materials to high temperatures promotes the precipitation of deleterious intermetallic phases that cause significant damage to the mechanical and corrosion properties of these materials. In this study, the UNS S31803 duplex stainless steel received a thermal treatment at a temperature of 830 °C for 30, 90, and 180 minutes. After the treatment, the precipitates were characterized by backscattered electrons (BSE) and chemical composition mapping, and the properties of impact toughness were assessed by Charpy V-notch test for the different treatment conditions. The corrosion resistance properties were assessed by cyclic potentiodynamic polarization study. The thermal treatments at 830 °C resulted in a considerable reduction of impact toughness, and the corrosion resistance was also reduced in longer treatment times along with the loss of the passivation ability of the materials treated.

Keywords: *duplex stainless steel, heat treatment, cyclic potentiodynamic polarisation, fracture toughness.*

1. Introduction

The duplex stainless steels (DSS) main characteristic is a microstructure made of two phases: austenite (γ), rich in nickel and nitrogen, and ferrite (α), rich in chromium and molybdenum. The fraction of each phase for these materials cannot be lower than 30% [1]. These materials may be produced by smelting, rolling, or forging with the final microstructural phase balance controlled by the chemical composition and the solubilization thermal treatment [1,2]. The optimum combination of mechanical strength and corrosion resistance provides these materials with a broad application field in the petrochemical industry, paper and cellulose industries, and marine environments.

However, the exposure of DSS to temperatures between 600 and 1000 °C induces the precipitation of intermetallic phases such as sigma (σ), chi (χ), and chromium nitride (Cr_2N). These phases cause significant damage to the toughness and corrosion resistance of duplex stainless steels [4,3,5]. The sigma phase is a ternary phase that consists of Fe-Cr-Mo, with low toughness and fragile behaviour [4,5,6]. The chi phase is a quaternary compound of Fe-Cr-Ni-Mo, with higher Mo content than that of the sigma phase. This phase has a higher atomic weight, and it is formed first, acting as a nucleation site for the posterior precipitation of sigma [5,6]. The Cr_2N phase may also be formed during the thermal treatment, but in a slightly lower fraction than chi and sigma phases [7,8].

The duplex stainless steels present high impact toughness when solubilised, but with the formation of intermetallic phases such as Cr_2N, chi, and sigma, the toughness values are affected [9,10]. Several studies [9,10,11] show that fractions of intermetallic phases lower than 1% are enough to reduce the toughness of duplex steels up to 50%. Therefore, a great effort is applied to reduce the formation of intermetallic compounds in duplex steels with a time of exposure at 600 to 1000 ºC temperature range to be especially avoided [12,13,14].

The corrosion resistance in duplex stainless steels is related to alloy elements such as Cr, Ni, Mo, and N [15,16]. The precipitation kinetics of the sigma phase is controlled by the diffusion of Cr and Mo in a eutectoid reaction, in which $\alpha \rightarrow \sigma + \gamma_2$. The values of Cr and Mo decrease in the regions adjacent to the formation of the σ phase, and this is the preferential area for corrosion [16]. The formation of galvanic pairs favours the dissolution of areas adjacent to sigma phase, and the sigma phase presents a cathodic effect concerning its vicinity in the presence of corrosive medium [6,17,18].

In this study, the performance of the UNS S31803 duplex steel was assessed after the ageing treatment at 830 °C for different exposure times of 30, 90, and 180 minutes. Different techniques evaluated the precipitation of intermetallic phases, and the Charpy impact toughness was analysed, with posterior fractographic analyses. Finally, corrosion resistance was assessed by potentiodynamic polarization in NaCl 1 mol.L^{-1} solution.

*e-mail: williamhaupt@upf.br.

2. Experimental Procedure

2.1 Thermal treatment

The thermal treatment applied in this study was performed in a muffle furnace without atmospheric control, (Jung, model 4212). The furnace was heated up to the ageing temperature of 830 °C, and the specimens were inserted and maintained for 30, 90, and 180 minutes followed by air cooling. The samples were identified as base metal (0), 30 minutes (30), 90 minutes (90), and 180 minutes (180).

2.2 Microstructural

The metallographic samples were prepared according to ASTM E 3 standard [19] procedures, as they were subjected to mechanical sanding with different grain sizes of P220, P400, P600, P1200, and P2000, and polishing with 6 µm, 3 µm, and 1 µm diamond paste.

The microstructure analysis was performed using a scanning electron microscope from Tescan, model Vega 3 LM, with backscattered electron (BSE) detector. The analyses of semi-quantitative chemical composition were performed using an energy-dispersive system (EDS), model Oxford Xmax. For image acquisition, the voltage parameters were standardized at 20 kV.

After the visual identification of the phases through the micrographic analysis via scanning electron microscopy (SEM), the samples were analysed with the help of the Phase Analysis software present in the light microscope Olympus, model BX51M; five images were assessed for each treatment condition.

2.3 X-ray diffraction analysis

X-ray diffraction patterns (XRD) were applied for phase characterization, using Cu-Ka radiation, acceleration potential of 30 kV and 30 mA filament current, at a rate of 0,04 deg/8 sec and a scan time of 5 hours.

2.4 Toughness properties

The Charpy impact test was performed according to the ASTM E 23 standard [20] with a 10x10x55 mm V-notch specimen, the equipment used was the Shenk, with the maximum capacity of 300 J, and all the samples were tested at the temperature of 25 °C ± 1 °C. After the tests, the fracture surfaces were analysed by SEM to verify the fracture mode.

2.5 Electrochemical measurements

The technique of cyclic potentiodynamic polarization was applied to evaluate the corrosion resistance in the base material and the different treatment conditions. The materials were embedded in epoxy resin, sanded, and polished with 1 µm alumina up to a specular surface; the edges of the sample were isolated with varnish to avoid crevice corrosion. The tests were performed in an aerated NaCl 1 mol.L^{-1} solution in triplicates, using a platinum counter electrode, Ag/AgCl reference electrode, and the specimen with an exposed area of 1 cm^2 (working electrode). The equipment used was a METROM AUTOLAB potentiostat, model PGSTAT128N, scanning from -400 mV (cathodic region) at a scanning rate of 1 mV/s. The tests were performed up to a current density (j) of 1 mA.cm^{-2}, and after reaching this value, the potential was reversed toward the initial potential. The corrosion surfaces were assessed by SEM for the analysis of the corroded surfaces.

3. Results and Discussion

3.1 Base material characteristics

The material investigated in the present study is the UNS S31803 duplex stainless steel, with its chemical composition obtained by an optical emission spectroscopy, presented in Table 1.

Figure 1 shows the microstructure of the as-received material, which was solubilized at 1080 °C and water quenching.

3.2 Microstructure characterisation

Figure 2 shows the microstructure of the UNS S31803 in the as-received condition and after ageing at 830 ºC for the delimited times. The phases formed during the ageing treatment were analysed via SEM in BSE mode. The increase in the atomic weight of the phases increases the backscatter coefficient (η) proportionally, according to the Monte Carlo model, so that the phases with higher atomic weight present a brighter image and phases of low atomic weight seem dark in contrast to the matrix [21].

In the DSS, the contrast among grey scales allows distinguishing the phases of ferrite (α) or austenite (γ) in the matrix, as could be shown in Figure 2 (A). It is also possible to distinguish the formed precipitates. The chi (χ) phase, which is composed of Fe, Cr, and a high content of Mo, presents higher atomic weight than the other phases, thus producing a whitish shade. In contrast, the sigma (σ) phase presents a light-grey shade, being composed by Fe, Cr, and a lower amount of Mo than those present in the χ phase, having a lower atomic weight. Additionally, black spots may be visualised in the matrix, which are phases of low atomic weight, potentially chromium nitrides.

Table 1. Chemical composition of the duplex as received material.

Material	Classification	C	Si	Mn	P	S	Cr	Ni	Mo	N
Base material	UNS S31803	0.016	0.363	1.59	0.011	<0.0010	21.8	4.95	2.74	0.225

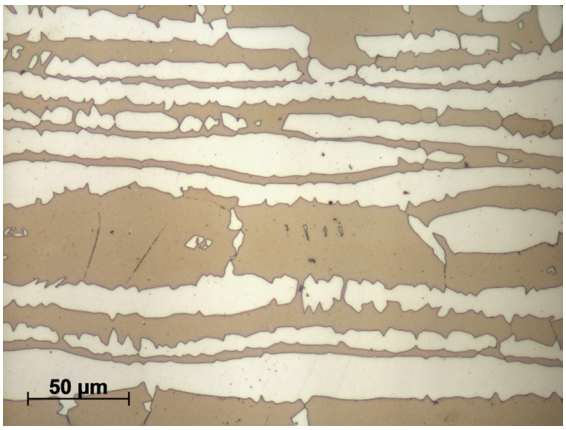

Figure 1. Microstructure of the as received material. Optical Microscopy. Modified Behara Etchant.

The formation of small light spots was visible in the austenitic edges compatible with the chi phase, and the presence of dark spots in ferrite phase, indicating the potential formation of nitrides is also visible in the condition treated for 30 minutes - Figure 2 (B)

The increase in chi phase may be seen along the edges of the austenitic grain in the 90-minute treatment - Figure 2 (C); there was also the decomposition of the ferrite phase with the formation of sigma phase and presence of secondary austenite. On the other hand, in the 180-minute treatment - Figure 2 (D), a significant increase in the fraction of the sigma phase in a lamellar morphology along the ferrite was observed, and the presence of the chi phase was verified along the austenitic edges, as well as a more prominent decomposition of the ferrite matrix.

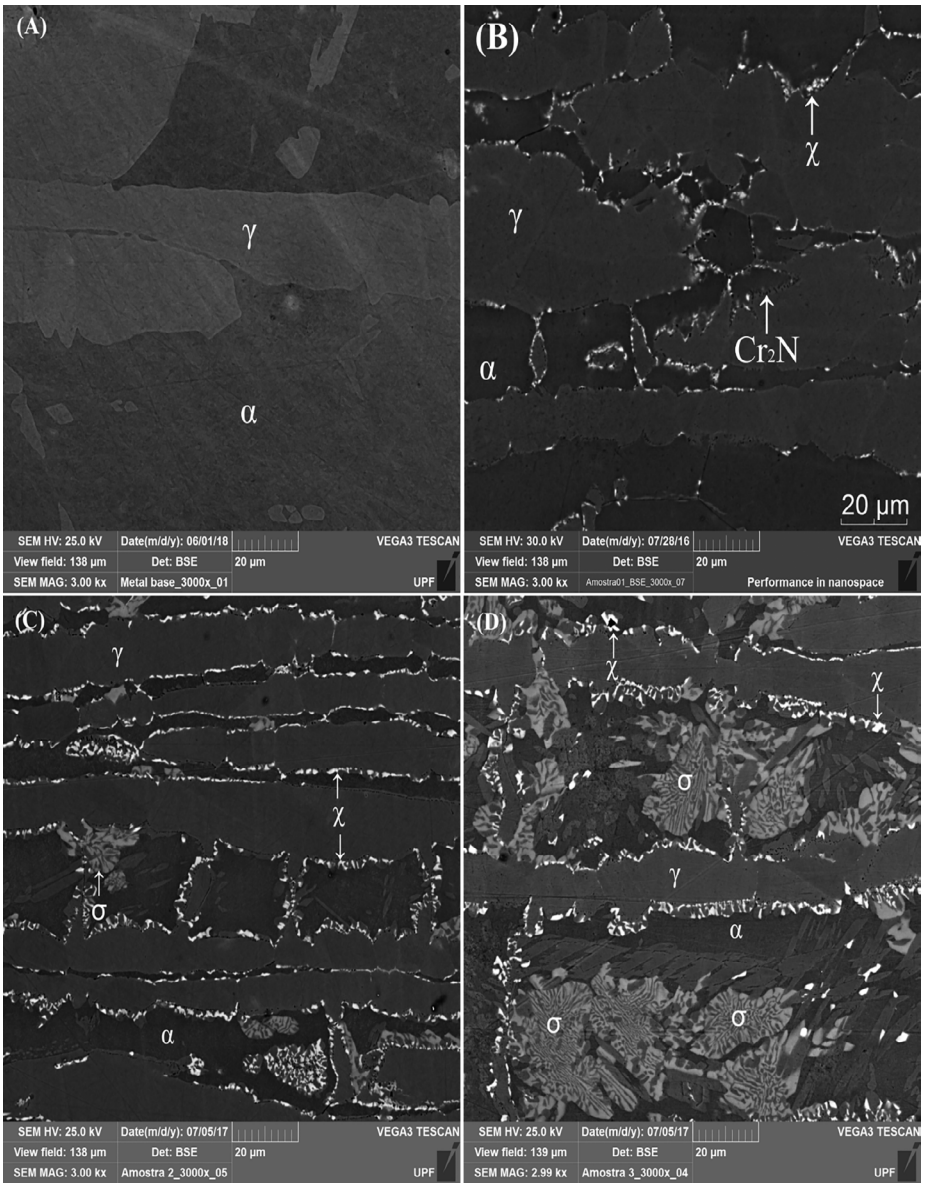

Figure 2. SEM micrographs in BSE mode: (A) As-received material, (B) Ageing at 830C for 30 minutes, (C) Ageing at 830C for 90 minutes, and (D) Ageing at 830C for 180 minutes.

3.3 EDS analyses maps

In Figure 3 (30-minute ageing treatment), overall, the scattering of chemical elements is identified in virtually the entire sample, but the elements are more concentrated in some regions. Iron (Fe) is scattered more homogeneously in the entire microstructure, the chromium (Cr) element is more concentrated in the α phase, and nickel (Ni) is found within the γ phase. Molybdenum (Mo) is scattered in the structure, but in higher concentrations in the lighter phase, corroborating the results presented in the image of Figure 2 in (B), which provides more indications of the presence of the Chi (χ) intermetallic phase. According to Paschoal et al. [14], the Chi phase is more abundant in molybdenum rich regions, and its identification is possible through the EDS analysis with differential contrast by the higher atomic mass of this element in the nominal composition of the duplex steels.

The 90-minute treatment allowed visualizing the formation of the Chi phase and the beginning of the Sigma phase formation. It is known that the interface of the χ phase is the main nucleation site of the Sigma phase. The Mo and Cr contents in the Sigma phase were higher than those presented by the α/γ matrix. This phenomenon may be associated with the decomposition of α for the formation of the Sigma phase, and the remaining α phase is weakened in Cr and reinforced in Ni, which may turn into secondary austenite. Figure 4 presents this condition.

Figure 5 shows the 180-minute treatment condition with a homogeneous Fe distribution in the matrix. It was also identified an increment in the concentration of Cr and Mo in the remaining Chi phase, but especially in the Sigma phase, which assumed the highest concentration of these chemical elements in these phases.

Table 2 allows visualizing the amount of the chi and sigma phases at the different treatment times. The phase fraction was measured using image analysis techniques with images obtained in SEM with backscattered electrons mode. The formation of the chi phase may be seen for the 30-minute treatment, and the increased formation of the chi phase and the formation of the sigma phase may be seen in the 90-minute treatment condition for the 180-minute condition, the fraction of chi phase is slightly reduced with the increase of sigma phase values.

The phase fraction present in the image of molybdenum mapping is presented in Table 3. The values obtained in the counting of Chi + sigma phases were somewhat similar, confirming the similarity and agreement between both analysis methods.

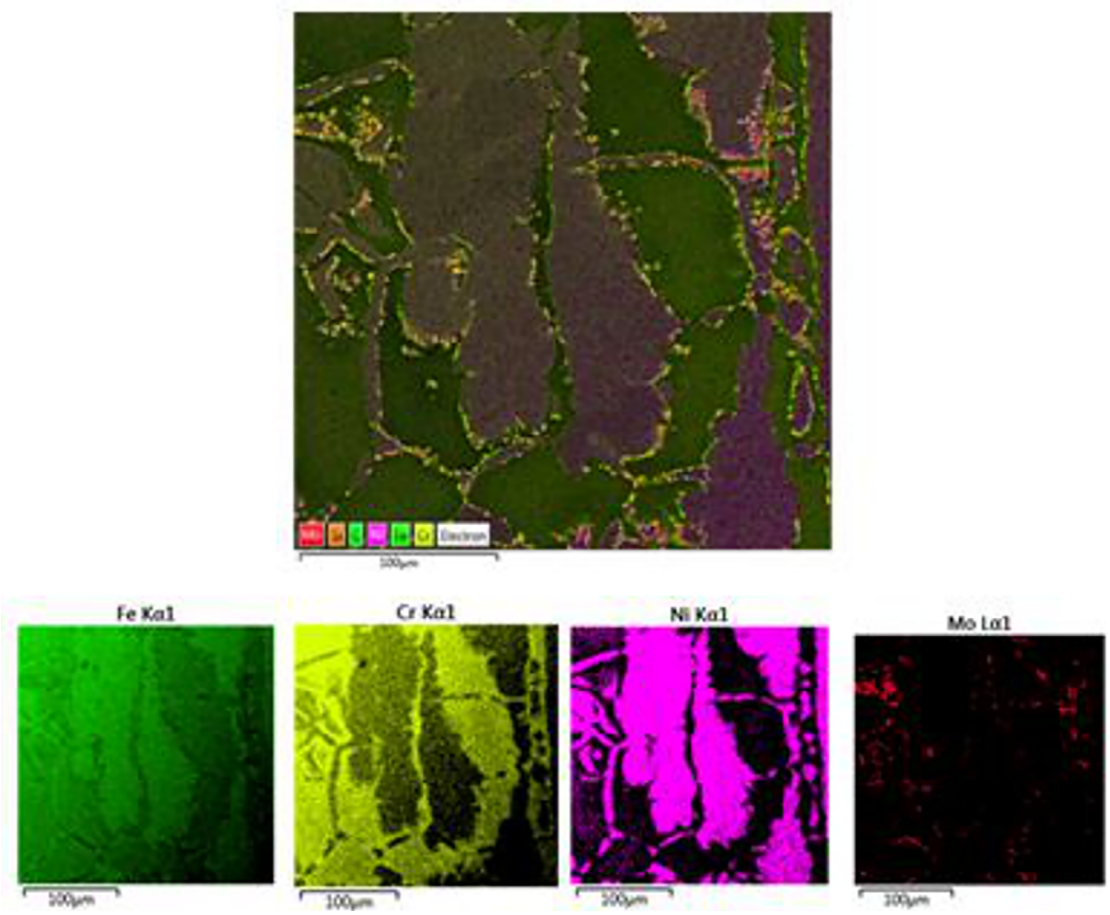

Figure 3. EDS compositional mapping for sample aged at 830C for 30 minutes.

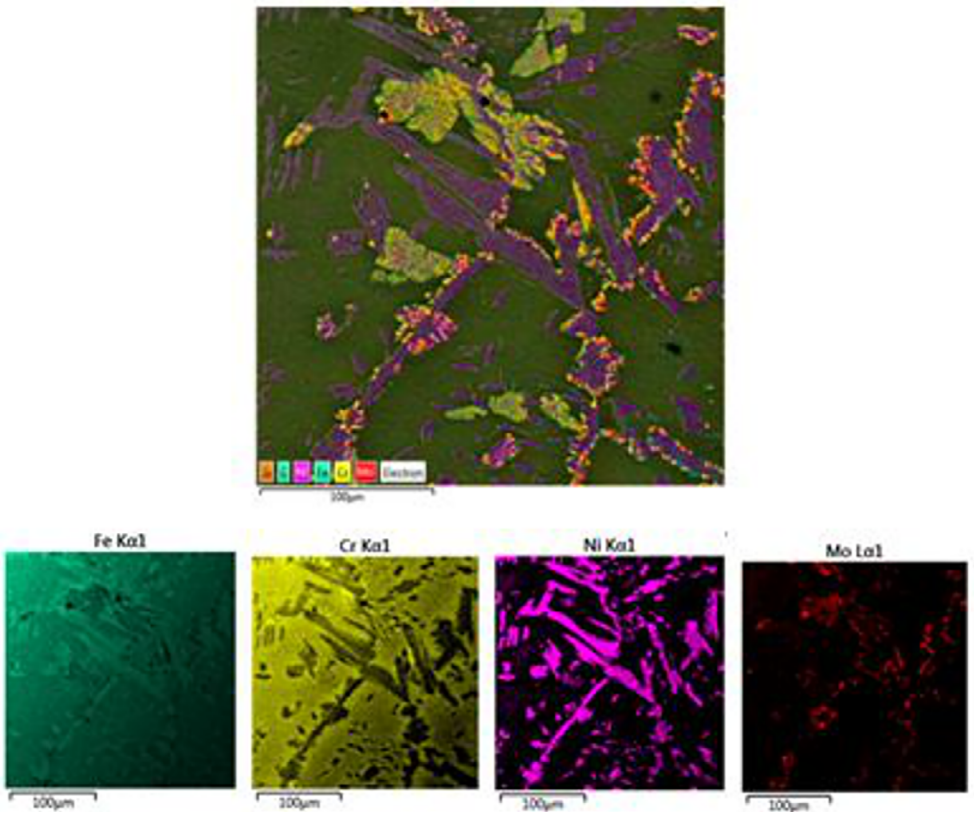

Figure 4. EDS compositional mapping for sample aged at 830C for 90 minutes.

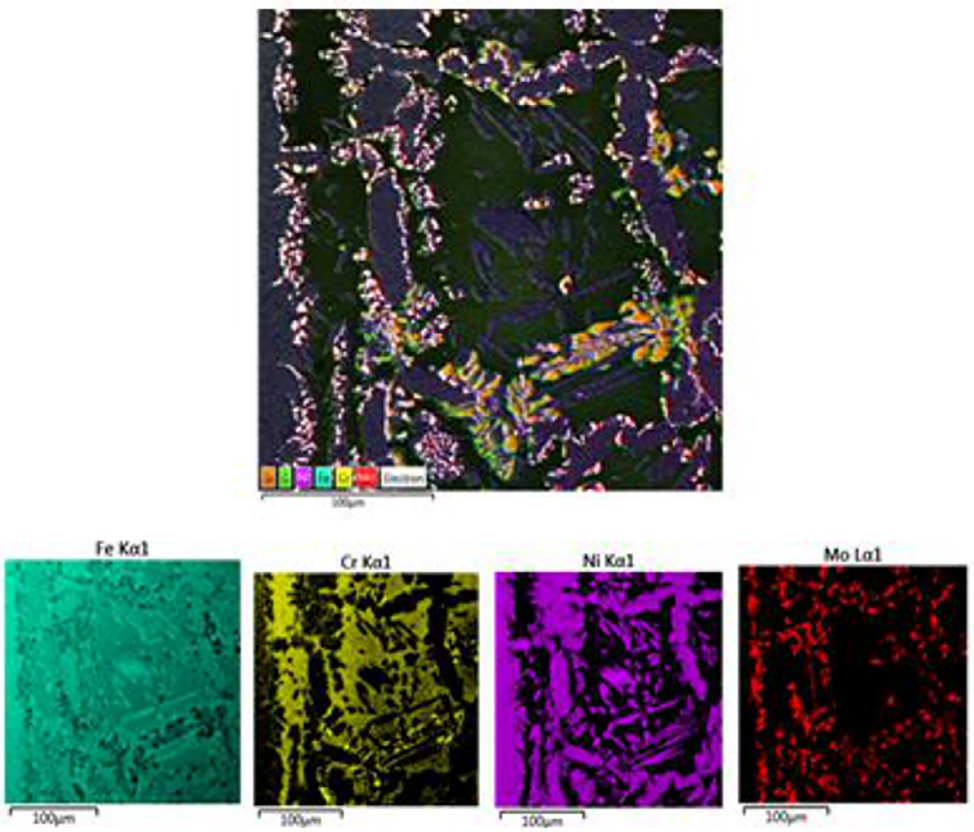

Figure 5. EDS compositional mapping for sample aged at 830C for 180 minutes.

Table 2. Amount of chi and sigma phases measured by image analysis for the ageing at 830 ºC for different times.

Treatment	**30**		**90**		**180**	
BSE phases	Chi		Chi+Sigma		Chi+Sigma	
Mean %	1.468		13.536		18.05	
BSE phases	Chi	Sigma	Chi	Sigma	Chi	Sigma
Mean %	1.468	-	2.7	10.836	2.62	15.43
Standard Deviation	0.52	-	0.5	1.62	0.58	2.85

Table 3. Amount of chi and sigma phases for the different treatment conditions, as measured by the counting method from EDS mapping images, method image analysis.

Treatment	**30**	**90**	**180**
Phase maps	Chi	Chi+Sigma	Chi+Sigma
Mean %	2.1	13.57	16.7
Standard Deviation	0.096	0.61	1.16

3.4 X-ray diffraction analysis

The presence of sigma phase is confirmed for the treatment conditions of 30, 90 and 180 minutes, as identified in the diffractograms presented in Figure 6 (B, C and D). The presence of Cr_2N is also observed in the diagrams. The chi phase is superimposed on the Cr_2N peaks, making it difficult to identify them for fractions smaller than 5%. The chi phase can be differentiated from the Cr_2N and sigma phases by the presence of high levels of Mo recorded in the evaluations with EDS maps, and the Cr_2N phase presents as dark spots in the BSE images due to their low atomic weight. The as-received material indicated only the formation of ferrite and austenite, according to Figure 6 (A). With the identification of the X-ray peaks it is possible to verify the increase of the percentages of sigma phase for the conditions of 90 and 180 minutes, it is also possible to verify a higher intensity of the peak of phase chi in the condition of 90 minutes with a slight reduction in the formation of this phase for 180 minutes of treatment, with significant increase in the percentage of sigma phase.

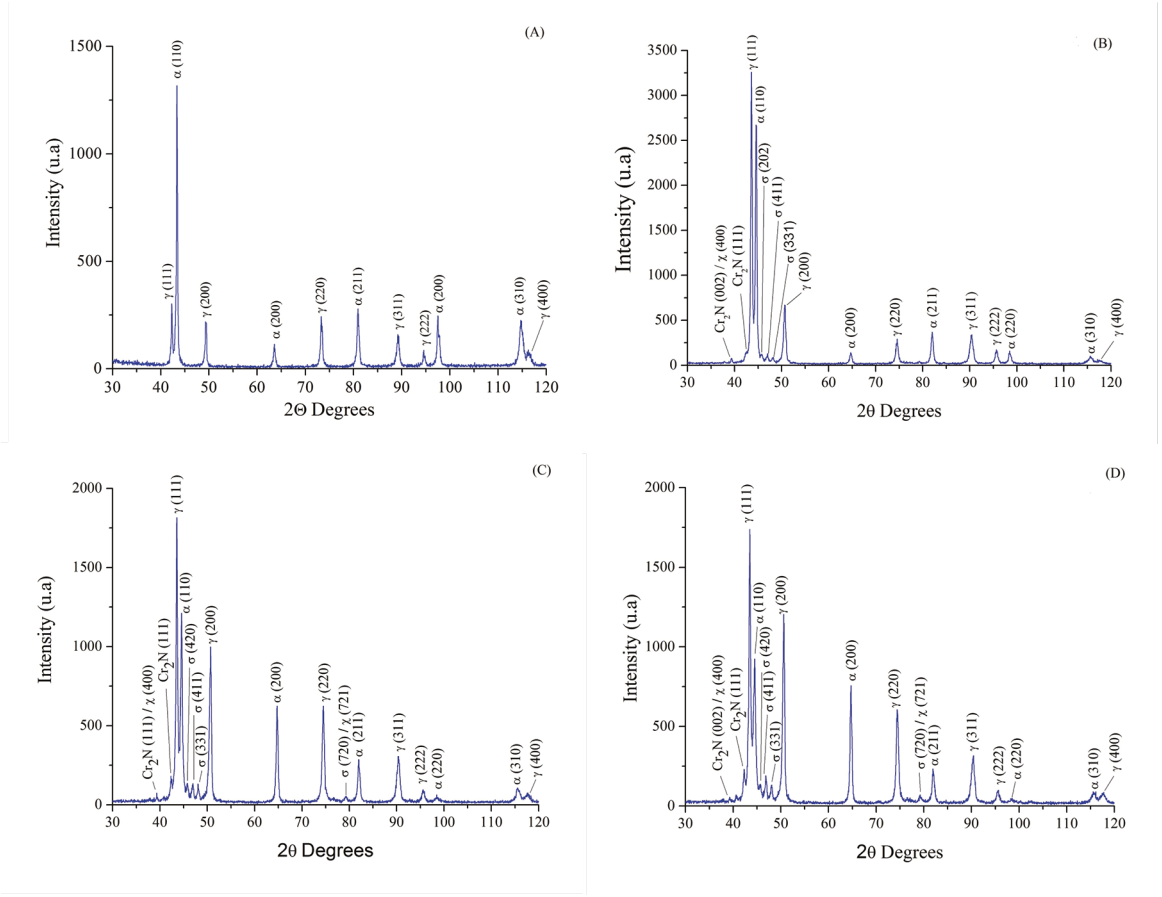

Figure 6. Diffractograms samples A) As-received, B) 30 minutes, C) 90 minutes and D) 180 minutes.

3.5 Impact toughness

The impact toughness of the UNS S31803 duplex steel material in the solubilized condition reached a mean value of 297 Joules. As expected, duplex stainless steels present high impact energy values due to their alternated microstructure composition of the γ/α phases. Figure 7 shows the influence of different ageing times at 830 °C on toughness and fracture mode of the duplex steel. In the condition as-received Figure 8, the material showed high impact tenacity with ductile fracture and predominance of dimples on its fracture surface. For the 30-minute treatment condition, a considerable reduction of impact toughness values was recorded, with a mean value of 39 J, the prevalent fracture mode was cleavage, and some points showed the presence of dimples, as presented in Figure 8A. The mean impact energy for the 90-minute treatment condition was 19 J, and the standard fracture mode was cleavage Figure 8B. The 180-minute treatment condition presented mean toughness of 14 J, and the fracture surface presented cleavage with fragile behaviour Figure 8C. The impact results indicate that even for a 2.1% fraction of precipitates as recorded for the 30-minute treatment condition, the fracture toughness is somewhat affected, with reduction of 86% for this condition in comparison with the as-received material.

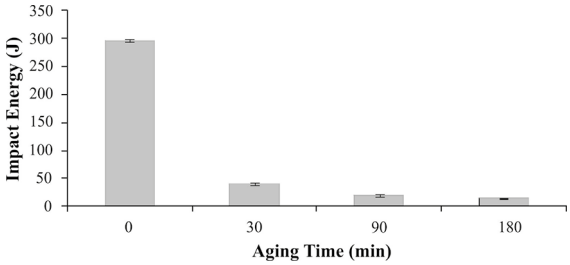

Figure 7. Charpy impact energy as a function of ageing time at 830 ºC.

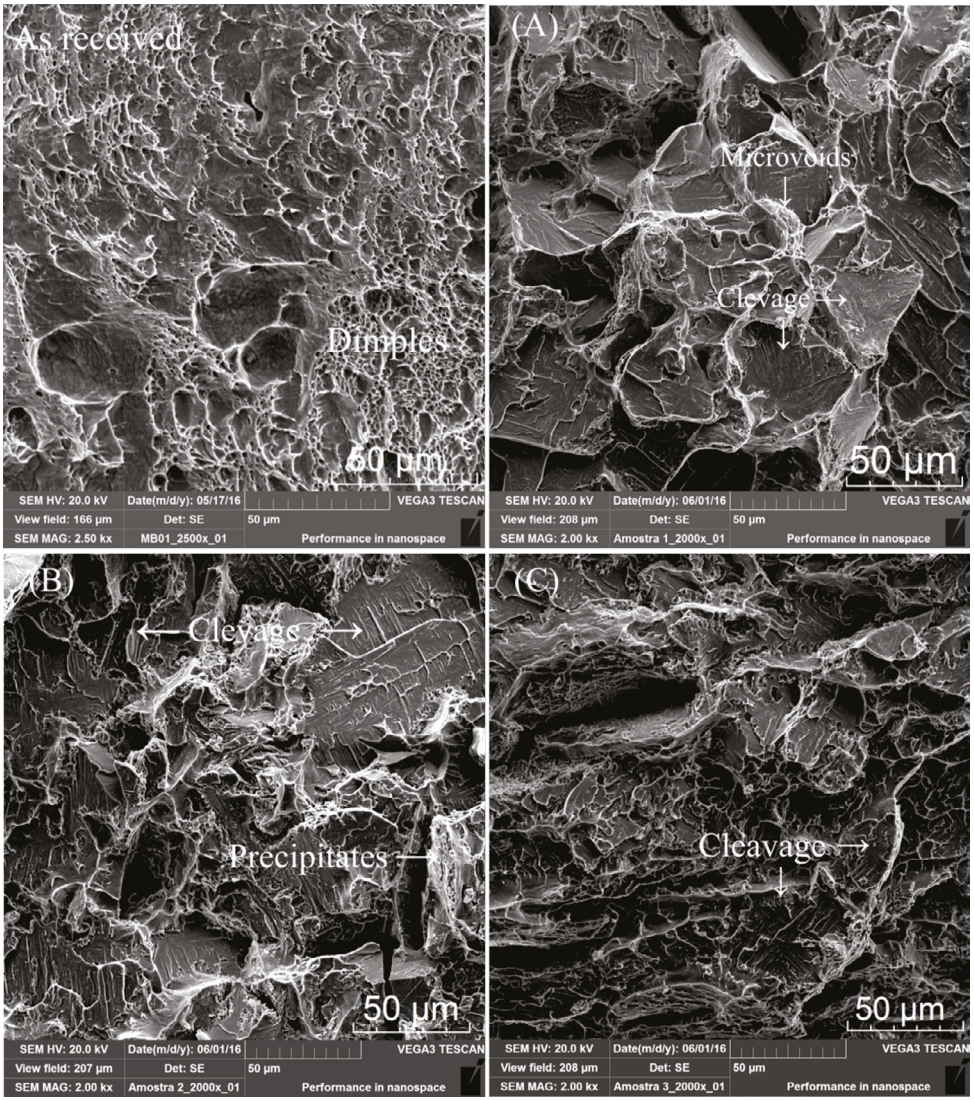

Figure 8. Impact Charpy V notch fracture surface images for ageing at 830 ºC for different times. Asreceived, A) 30 minutes, B) 90 minutes, and C) 180 minutes.

Longer ageing times, promoting more significant fractions of χ phases and formation of sigma phase, resulted in 93% and 95% reductions in impact strength for the 90 and 180-minute treatment conditions, in comparison to the toughness of the as-received material; the mean amount of precipitated phases for the respective conditions are 13.53% and 18.05%. A study performed by Calliari et al. [10] recorded reductions of 50% in impact toughness with the presence of 0.5% of precipitated phases. For precipitation values of 2%, there was even more significant damage in fracture toughness with small ductile fracture points, and for precipitation values between 6% and 8%, the fracture occurred by cleavage in the entire surface.

3.6 Cyclic potentiodynamic polarisation

The base material in the as-received condition (As-received) presented pitting formation with passivation for the three samples tested. In contrast, the curves for the conditions thermally treated presented large hysteresis during the return of the cyclic voltammetry, without presenting the phenomenon of passivation as could be seen in Figure 9.

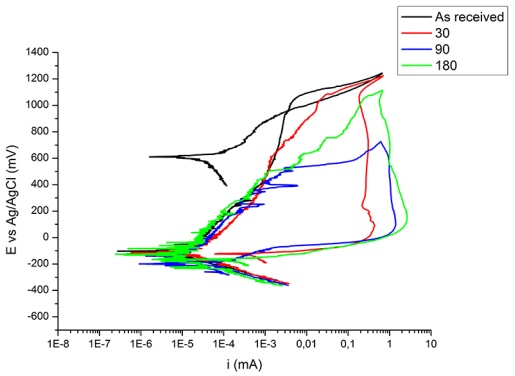

Figure 9. Potentiodynamic polarization curves specimens after as-received, 30, 90 and 180 minutes ageing at 830 ºC.

The corrosion potentials presented a small variation for the different conditions assessed, showing a low influence of the thermal treatment on the surface equilibrium state in the corrosive medium. The same behaviour may be observed for the region of passive currents, which showed a quite similar result among the different ageing times. The pitting potentials presented considerable variation with the different treatments, and it was possible to verify a metastable pitting formation for the 180-minute condition, with a substantial reduction in pitting potential in comparison to the as-received condition.

Table 4 shows the results of corrosion potential (E_{corr}), pitting potential (E_{pit}), and (E_{corr}-E_{pit}).

Figure 10 shows sample surfaces after the polarisation tests indicating pitting formation for the as-received condition Figure 10, while the condition treated for 30 minutes showed corrosion in the edges of the precipitates Figure 10A. For the 90-minute treatment condition

Table 4. Corrosion and pitting potentials and electrical work during polarisations for the different ageing condition evaluated.

Aging time	E corr (mV)	E pit (mV)	Ecorr – Epit (mV)
0	-134.3±47.5	1169±6.0	-1303.3
30	-133.3±78.7	1165±4.3	-1298.3
90	-144.3±55.7	669±14.0	-813.3
180	-186.3±15.5	549±22.8	-735.3
	E repassivation		
0		1121.3±12.8	

Figure 10B, the corrosion was enhanced in the region of precipitates, and in the 180-minute condition Figure 10C, there was a slightly aggressive attack to the region near the precipitates, confirming strong intergranular corrosion promoted by the decrease on alloy content at the vicinity of precipitates.

4. Conclusions

The study showed the initial formation of the chi and nitride phases at 30 minutes, exposing the formation of the sigma phase only at 90 and 180 minutes of the 830 C ageing treatment.

The EDS mapping of the precipitated phases reinforces the finding of precipitation of the chi phase due to the high Mo content and of the sigma phase due to the higher values of Cr and Mo present along with these phases.

For the 830 ºC ageing treatment for 90 and 180 minutes, the fraction of precipitated phases was 11% and 12.4% with a reduction of 93% and 95% in toughness values when compared to the as-received material.

From the XRD analyses, it is possible to confirm the presence of sigma phase for all the treatment conditions.

The presence of the Cr_2N and chi phases can also be identified for the treated conditions, and their identification is possible together with the MAP and BSE analyses.

It may be verified that the thermal treatment at 830 °C has a deleterious effect on the toughness of the UNS S31803 alloy, while at exposure times of 30 minutes with 3.2% of precipitated phases the reduction of toughness values as 86% in comparison to the as-received condition.

The fracture micromechanism observed for the different ageing conditions were predominately cleavage in the 30-minute treatment condition and cleavage for the 90 and 180-minute treatment conditions.

The corrosion resistance in the 30-minute treatment condition presented corrosion potential and pitting potential somewhat similar to the as-received, but the intergranular corrosion observed in the 30-minute treatment condition was sufficient to inhibit the passivation of the material.

For the 90 and 180-minute treatment conditions, there was an accentuated decrease in pitting potential in comparison to the as-received material, with a reduction of 42.8% and 53.03% in pitting potential, respectively.

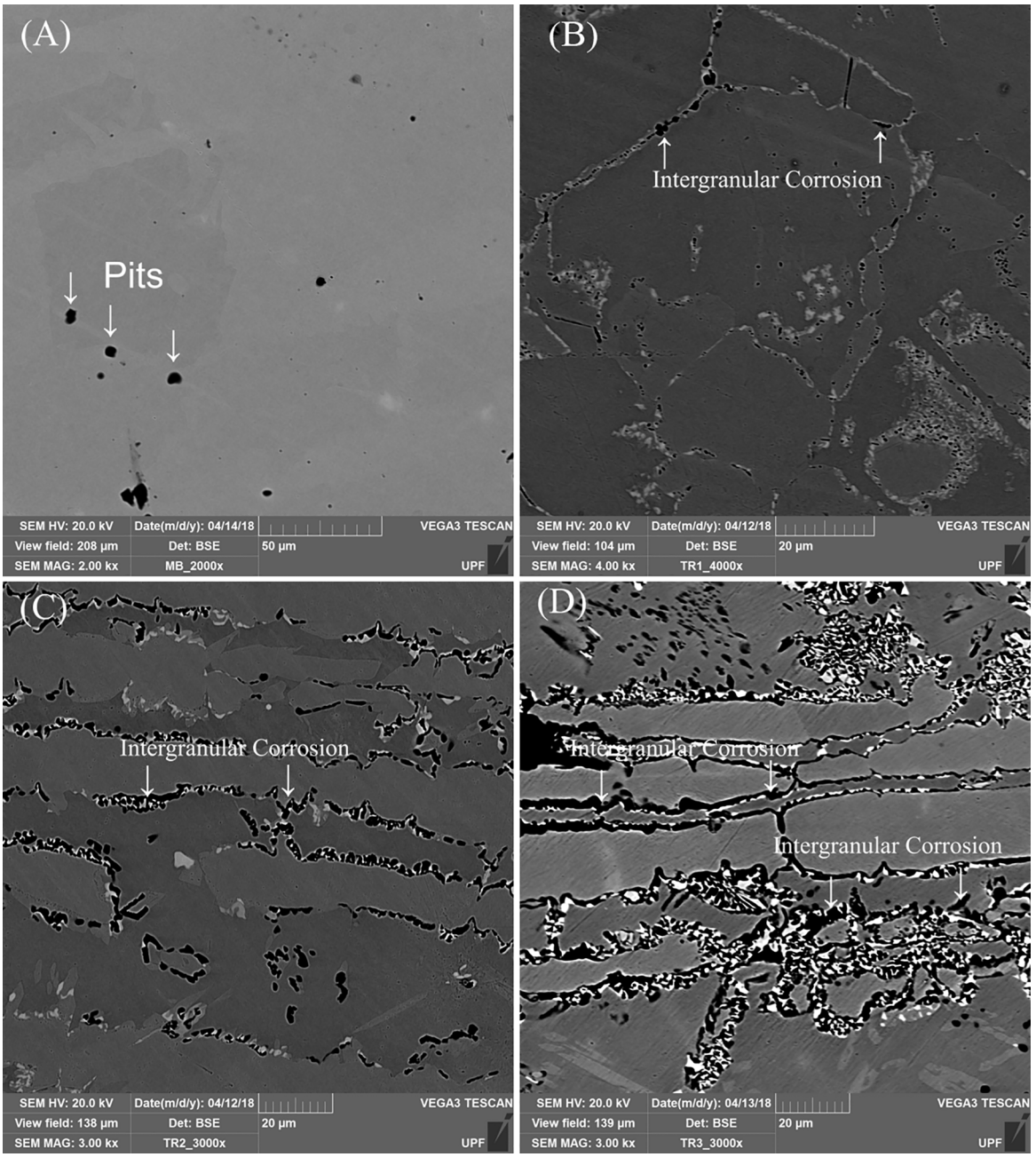

Figure 10. Surfaces after the polarisation test for ageing at 830 ºC for different times. As-received, A) 30 minutes, B) 90 minutes, and C) 180 minutes.

5. Acknowledgements

The authors would like to acknowledge CAPES for its financial support.

6. References

1. Gunn RN. *Duplex stainless steels – microstructure, properties and applications*. Cambridge: Woodhead Publishing; 1997.

2. Outokumpu O. *Handbook of stainless steels*. Finland: Outokumpu Oyj; 2013.

3. Nilsson JO, Wilson A. Influence of isothermal phase transformations on toughness and pitting corrosion of super duplex stainless steel SAF 2507. *Materials Science and Technology*. 1993;9(7):545-54.

4. Lee JS, Kim IS, Kimura A. Application of small punch test to evaluate Sigma-phase embrittlement of pressure vessel cladding material. *Journal of Nuclear Science and Technology*. 2003;40(9):664-71.

5. Ahn JH, Jung HD, Im JH, Jung KH, Moon BM. Influence of the addition of gadolinium on the microstructure and mechanical properties of duplex stainless steel. *Materials Science and Engineering: A*. 2016;658:255-62.

6. Yang SM, Chen YC, Chen CH, Huang WP, Lin DY. Microstructural characterisation of δ/γ/σ/γ2/χ phases in silver-doped 2205 duplex stainless steel under 800 C ageing. *Journal of Alloys and Compounds*. 2015;633:48-53.

7. Santos DC, Magnabosco R. Kinetic study to predict sigma phase formation in duplex stainless steels. *Metallurgical and Materials Transactions: A*. 2016;47(4):1554-65.

8. Magnabosco R. Kinetics of sigma phase formation in duplex stainless steel. *Materials Research*. 2009;12(3):321-27.

9. Kim JH, Oh EJ, Lee BC, Kang CY. Effect of aging treatment on impact toughness and corrosion resistance of super duplex stainless steel. *Journal of Materials Engineering and Performance*. 2016;25(1):9-14.

10. Calliari I, Breda M, Ramous E, Magrini M. *Effect of isothermal heat treatments on duplex stainless steels impact toughness*. In: Convegno Nazionale IGF XXII. Roma, Italia; 2013 jul 1-2. Roma, Italia: IGF; 2013. p. 56-65.

11. Topolska S, Labanowski J. Effect of microstructure on impact toughness of duplex and super duplex stainless steels. *Journal of Achievements in Materials and Manufacturing Engineering*. 2009;36(2):142-9.

12. Santos DC, Magnabosco R, Moura-Neto C. Influence of sigma phase formation on pitting corrosion of an aged UNS S31803 duplex stainless steel. *Corrosion*. 2013;69(9):900-11.

13. Chan KW, Tjong SC. Effect of secondary phase precipitation on the corrosion behaviour of duplex stainless steels. *Materials*. 2014;7(7):5268-304.

14. Paschoal MB, Romana R, Magnabosco R. Quantificação de fases intermetálicas em aço inoxidável superdúplex por estereologia quantitativa – Efeito de diferentes fontes de imagens. *Tecnologia em Metalurgia, Materiais e Mineração*. 2015;12(4):310-7.

15. Chaves DS, Cardoso Junior R, Bracarense AQ, Frankel GS, Lins VFC. Cyclic polarization study of thick welded joints of lean duplex stainless steel for application in biodiesel industry. *Materials Research*. 2017;20(1):161-7.

16. Del Abra-Arzola JL, García-Rentería MA, Cruz-Hernández VL, García-Guerra J, Martínez-Landerosa VH, Falcón-Franco LA, et al. Study of the effect of sigma phase precipitation on the sliding wear and corrosion behaviour of duplex stainless steel AISI 2205. *Wear*. 2018;400-401:43-51.

17. Symniotis E. Galvanic effects on the active dissolution of duplex stainless steels. *Corrosion*. 1990;46:2-12.

18. Tsai WT, Chen JR. Galvanic corrosion between the constituent phases in duplex stainless steel. *Corrosion Science*. 2007;49(9):3659-68.

19. American Society for Testing and Materials (ASTM). *E3-01 – Standard guide for preparation of metallographic specimens*. West Conshohocken, PA: ASTM; 2001.

20. American Society for Testing and Materials (ASTM). *E23-07a – Standard test methods for notched bar impact testing of metallic materials.* West Conshohocken, PA: ASTM; 2011.

21. Goldstein J, Newbury DE, Joy DC, Lyman CE, Echlin P, Lifshin E, et al. *Scanning electron microscopy and X-ray microanalysis*. 3rd ed. New York: Springer US; 2003.